31st Congress of the International Council of the Aeronautical Sciences

Belo Horizonte, Brazil; September 09-14, 2018

TIME-RESOLVED PRESSURE MEASUREMENTS FOR AN AIRFOIL WITH SELF-SUSTAINED SHOCK OSCILATIONS

Henrique Fanini Leite*, Roberto Gil Annes da Silva* and Ana Cristina Avelar**
***ITA – Instituto Tecnológico de Aeronáutica, **IAE – Instituto de Aeronáutica e Espaço**

Keywords: *Pressure Sensitive Paint, Buffeting, Transonic Flow*

Abstract

In order to understand the mechanisms behind self-sustained shockwave oscillations under laminar flow, the pressure distributions over a NACA 0012 airfoil with free transition were measured using two types of fast-response pressure-sensitive paints. The airfoil was submitted to flow near and at buffeting conditions. Pressure fields were analyzed using Power Spectral Density (PSD), Cross Power Spectral Density (CPSD) and pressure time-series standard deviation, as well as general flow visualization. Results indicate a clear shockwave oscillation frequency which does not match its turbulent flow counterpart. In addition, CPSD phase shift analysis allows the identification of different regions of shockwave interaction.

1 Introduction

In modern-day supercritical airfoils, large amplitude shockwave oscillations represent a serious performance limitation both in terms of maximum allowed flight Mach number and maximum angle of attack [1]. In addition to shockwave induced buffeting, several cases of structural limit cycle oscillations (LCO) have been associated to shockwave oscillations [2]. Due to its practical importance in aircraft design and flight safety, as well as costly and risky flight testing, several attempts were made at developing buffet prediction methods, to varying degrees of success [3]. The development of CFD codes has seen strong evolution along the years, and it is now possible to predict airfoil shockwave oscillation frequency and buffet boundaries reasonably well for some cases. Challenges remain in applying numerical simulations to real-world applications, however [4].

Shockwave oscillations were first described more than seventy years ago [5] and today there is already a strong empirical research base on the phenomenon, especially for turbulent flow [6]. However, the mechanisms behind shockwave oscillations are not completely understood. Work relating shockwave oscillations to interactions with the boundary layer was published by Pearsey, which described shock-induced bubble separation and trailing edge separation, as well as how pressure disturbances downstream of the shock can induce shock oscillations [7]. This work has been extended by Mundel and Mabey, who proposed the classification of shockwave boundary layer interactions (SBLI) in three types, depending on the level of surface pressure excitation [8].

A framework for characterization of shockwave oscillations was proposed in the classical paper by Tijdeman, who used an oscillating flap to induce shock oscillations under different flow velocities, and was able to identify three types of motion [9]. More recently, Lee has proposed an acoustic feedback mechanism to explain the phenomenon, according to which disturbances propagate from the shock to the trailing edge in the form of pressure waves in the separated flow region. On reaching the trailing edge, the disturbances generate upstream moving waves that impart energy to the shock, thus completing the cycle. Oscillating frequencies calculated with this method have agreed with experimental measurements [10].

Unfortunately, almost the entire body of literature regarding shockwave oscillations deals with the turbulent boundary layer case. In addition, there are notable differences between SBLI for the turbulent and laminar boundary layer cases, some of which have been known since the late forties [11]. Therefore, it is likely that shockwave oscillations will not behave in the same manner under a laminar boundary layer flow.

In one of the few references available, Dor et al. [12] did not detect any coherent buffet in supercritical airfoils under laminar flow. McDavit and Okuno, in their systematic NACA0012 buffet measurements, have also stated that under Reynolds below six million the oscillations were invariably erratic. There was no attempt at fixing the boundary layer transition, but qualitative analysis with thin oil film indicted a transition for Reynolds between one and two million. At Reynolds above six million, pressure sensors at midchord and the trailing edge indicated buffet onset simultaneously, while below this value, the midchord sensor responded first [6]. Thus, the inability to detect a clear buffet frequency might be related to different types of SBLI, instead of the boundary layer condition.

Recent experiments performed by Brion et al. at ONERA were able to identify shock oscillation frequencies for a supercritical airfoil under mostly laminar flow (laminar up to the shock, at least). They have identified two oscillating frequencies, one of them lower than its turbulent counterpart, at $St = 0.05$, and the other much higher, at $St = 1$. The PSD peak at $St = 1$ was very sharp and this frequency was associated with oscillations at the bottom part of the shockwave. The low-frequency peak was weaker and was associated with oscillations of the shockwave as a whole. In addition to the variations in frequency, shockwave oscillations for the laminar case had lower amplitude [22].

The experiments concerned by this paper had two objectives: to evaluate the performance of a recently implemented *fast-PSP* measurement system and to investigate the phenomenon of shockwave oscillation under laminar boundary layer. Experiments based on temperature sensitive paint (TSP), conducted at the same wind tunnel at very similar flow conditions to the ones presented in here, have shown that the flow remains laminar up to the shockwave [13]. Time resolved surface pressure data was analyzed by a variety of methods, such as Power Spectral Density and Cross Power Spectral Density (CPSD). From the results, it is clear that self-sustained shockwave oscillations are present and have a well-defined frequency.

2 Experimental Setup

Tests were carried out at the Pilot Transonic Tunnel (TTP), at Instituto de Aeronáutica e Espaço (IAE). The TTP test section is 30cm wide, 25cm high and 80cm length, with slotted walls and 830W of power. The tunnel operates at a pressure range of 0,5 to 1,25 bars, and its nominal Mach number range is 0,2 to 1,3. It operates in a conventional, closed, continuous circuit, driven by a main compressor, combined with an intermittent injection system, which can operate for 30 seconds at maximum flow [14]. It allows the control of flow temperature with a precision of 0,1°C, while Mach number uncertainty is in the range of 0,001. For these tests, only the injection system was used, which allowed for a maximum Mach number of 0,81 at 0° angle of attack. This value was slightly reduced for higher angles of attack due to blockage. To enable this mode of operation, the TTP circuit was modified to an open configuration. Such operation mode was chosen to allow the induction of a smooth, linear flow acceleration, which was the first non-stationary condition measured with the fast-response PSP system and reported on a previous paper, where detailed schematics of the tunnel modifications and of the experimental setup are described [15]. In addition to a reduced maximum Mach number, this configuration has led to an increased Mach number uncertainty of 0,006.

Besides accelerated flow measurements, data was acquired under maximum Mach number conditions for angles of attack of 0°, 2° and 4°, under acquisition frequencies of 500Hz, 2000Hz and 3000Hz. Two types of paint were used: the polymer-based ISSI TurboFIB and the Polymer-Ceramic ISSI PC-PSP. Both are optimized for time-resolved measurements, with

the former presenting good response characteristics for frequencies up to 1kHz, and the latter allowing measurements at up to 10kHz, according to the manufacturer [16, 17]. Experiment Reynolds Number was $Re = 1.10^6$. These paints were calibrated at the IAE calibration bench.

Image acquisition was done using a Speed Sense 9020 CMOS camera, controlled via trigger signal generated by a PSG-2 pulse generator. The pulse generator also commanded the water-cooled 400nm LED lamp. The cooling system had to be very stable, since variation of the LED temperature resulted in illumination intensity variations, which are an important error source. A 610nm long-pass filter was mounted on the camera lens, in order to filter out all light sources other than the PSP emission, in addition, a 400nm reflective coating was added to the filter, due to the strong illumination intensity. Acquired pictures were stored in the camera's internal memory and later transferred to the computer via Ethernet link. Depending on image size, up to 3000 pictures could be stored in the internal memory.

PSP tests were carried out on an intensity-based approach with single component paints. Despite the ability to mitigate some of the experiment error sources, a lifetime-based approach was impractical due to the unsteady conditions. Maybe a lifetime approach with very short time gates would work, but the low exposition period for each image would result in high noise levels and the necessity of two images for each condition would halve total acquisition time.

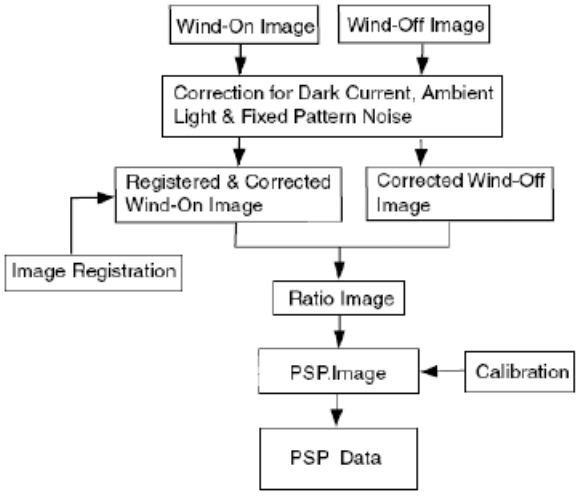

Fig. 1. PSP data reduction flowchart.

While for conventional PSP tests, with low volume of data, processing can be done in commercially available software [18], for larger test campaigns, and especially fast-PSP testing, specific processing algorithms must be developed, due to the large volume of data. This also allows for a much greater versatility in data reduction and manipulation, which is crucial for fast-PSP, since there is still no standard practice for unsteady PSP data reduction and post-processing.

Figure 1 provides the data reduction flowchart used in our experiments. Each of the represented steps was developed as a standalone MATLAB function. Thus, it is possible to combine them in any way, allowing great flexibility to the data processing algorithm. Images were acquired and processed according to the intensity method, in which wind-on images, taken at test conditions, and a reference image (also called wind-off image), taken at known reference conditions, are ratioed and related to Pressure according to a calibration curve. A background image was subtracted from all other images to eliminate the effects of external light sources. A detailed description of fast-response pressure sensitive paints and data reduction methods can be found in references [19] and [20]

Due to extensive available experimental data, a NACA0012 airfoil was chosen. It has 250mm span and 83mm chord and has five conventional pressure taps. The pressure taps transducers do not have a good frequency response, and could only be used to validate steady-state measurements. The experimental conditions analyzed in this paper are listed in table 1.

Table 1. Experiment Matrix

Condition	AoA	Mach
1	0°	0,80
2	2°	0,79
3	4°	0,77

3 Results and Discussion

All results presented in this paper were obtained using PC-PSP. While the manufacturer affirms that TurboFIB has a temporal response of up to 1 kHz, well within the necessary range to capture the oscillations, TurboFIB failed to capture the shockwave buffet in all test conditions. In fact, the TurboFIB temporal response is highly dependent on paint layer thickness [20]. Thus, the paint layer applied over the airfoil was probably too thick. A very thin paint layer, however, negatively impacts paint luminescence, and therefore its signal to noise ratio, and paint robustness. Moreover, it is very hard to control for paint layer thickness during manual painting procedures, which creates strong uncertainty regarding TurboFIB temporal response performance, or at least the repeatability of such performance characteristics.

According to literature data [6], experiment condition 3 is well within and condition 2 is very close to the buffet onset boundaries for a turbulent boundary-layer flow. Figure 2 presents the standard deviation of the pressure time series for the airfoil. Results are in good agreement with previous reports. Figure 2a, presenting data for the 0° AoA case presents low pressure fluctuations throughout the whole airfoil, with slightly higher values near the shockwave position. Red spots in the image represent image markers, which are used for image alignment. In figure 2b, presenting data for 2° AoA, low-intensity shock oscillations are visible. The shock line is not perfectly straight, indicating some degree of three dimensionality in the flow, caused by wall interference. The same interference is visible in figure 2c, presenting data for 4° AoA. In this condition, shockwave oscillations are clearly present and of higher amplitude and intensity. Besides the main shockwave, there is a region of increased pressure fluctuations upstream, which is caused by the first leg of a lambda-type shockwave. This type of structure is common in laminar flow and had been detected in several experiments with this same airfoil at TTP [13, 21].

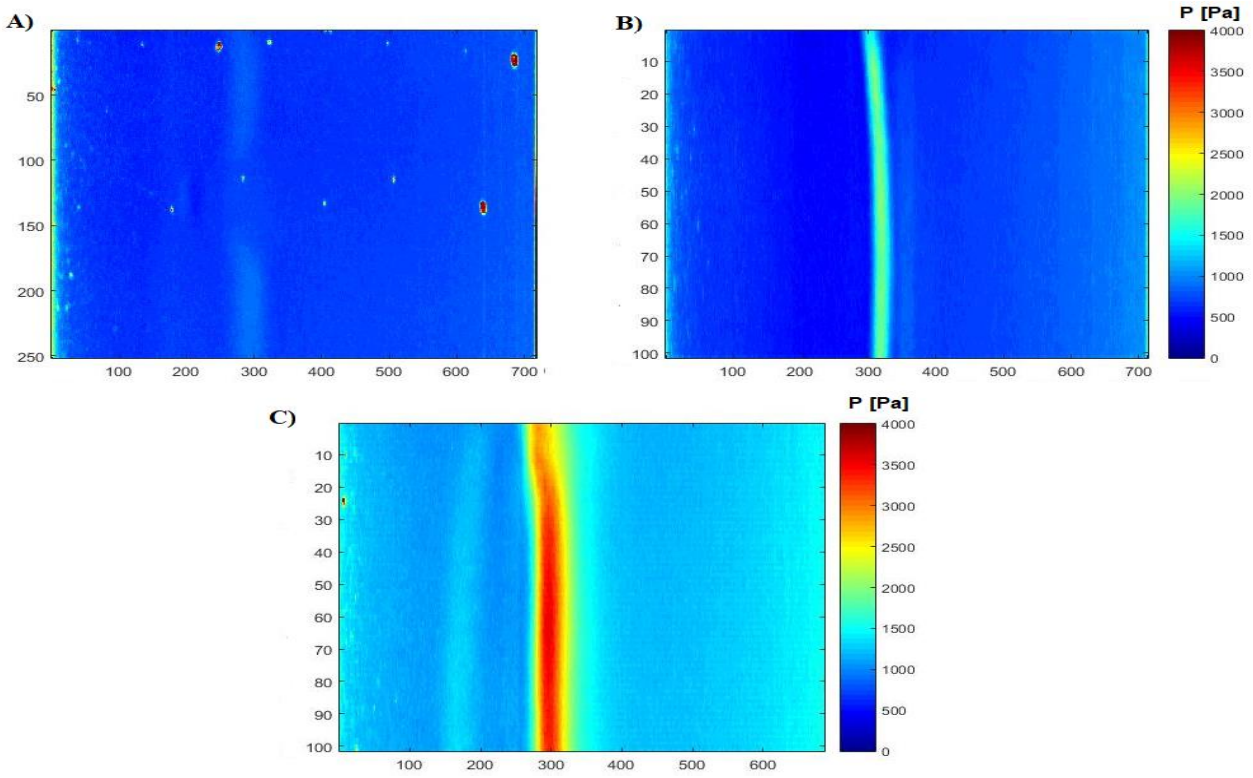

Fig. 2. Pressure standard deviation for the airfoil at angles of attack of A) 0°, B) 2° and C) 4°.

By averaging pressure values spanwise for each timeframe, it is possible to reduce

random noise. This allows more precise analysis of pressure fluctuation data. Figure 3 presents pressure fluctuation data, measured in a root mean square fashion, after spanwise averaging. Besides variations in shockwave oscillation intensity and amplitude, figure 3 reveals some interesting features. In all three cases, pressure fluctuations are markedly higher after the shock region and grow towards the trailing edge, indicating a probable boundary layer transition or separation. At two degrees of angle of attack, there is a distinct secondary pressure bump after the main shock region, which can be evidence of a post-shock bubble [1]. This structure is not present for the 4° case.

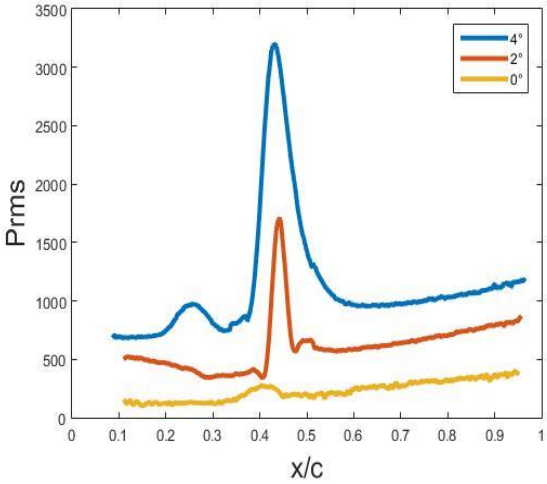

Fig. 3. Unfiltered chordwise pressure fluctuations.

Further evidence of the lambda type of flow can be seen in figure 4, which presents the same type of data for 0° and 2° after applying a 40Hz (semi-chord reduced frequency $k = 0{,}04$) high-pass finite impulse response (FIR) filter. Both curves present a bump upstream of the shock, which was overshadowed by low-frequency fluctuations, probably caused by injector-induced base flow instabilities.

The filtering procedure also makes the post-shockwave bump at 2° disappear. This behavior is at odds with what was reported by Mundel and Mabey [8], who described the bubble-induced pressure fluctuations as a high-frequency phenomenon. Another interesting feature is that even though pressure fluctuations downstream of the shock are still higher than upstream, high-pass filtering has considerably subdued the growth in pressure fluctuations towards the trailing edge for the 2° case, which did not happen to the 0° case. This indicates a broader spectrum for trailing edge pressure instabilities at 0°.

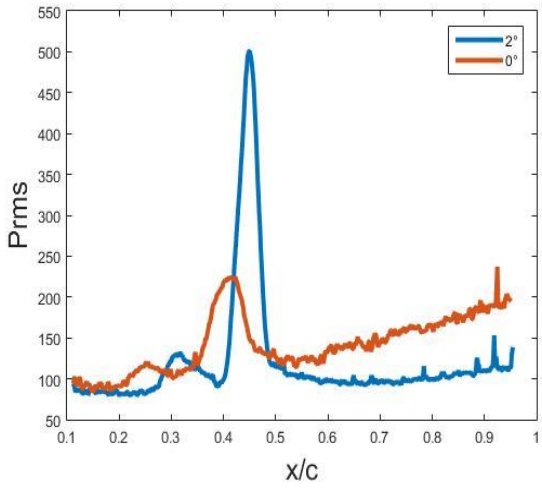

Fig. 4. High-pass filtered pressure fluctuations.

The shockwave oscillation frequency can be determined by FFT analysis. In order to eliminate low-frequency components, data was filtered through a 40Hz high-pass FIR filter. Results for the 4° case are presented in Figure 5. There is a clear peak at reduced frequency $k = 0.08466$. This corresponds to a frequency of 85Hz. These results do not match turbulent flow experimental data [6] or predictions based on Lee's method. As stated previously, reports on laminar flow shockwave oscillations are scarce, and tend to either fail to identify clear oscillation frequencies [12] or to report substantial differences between laminar and turbulent flow [22].

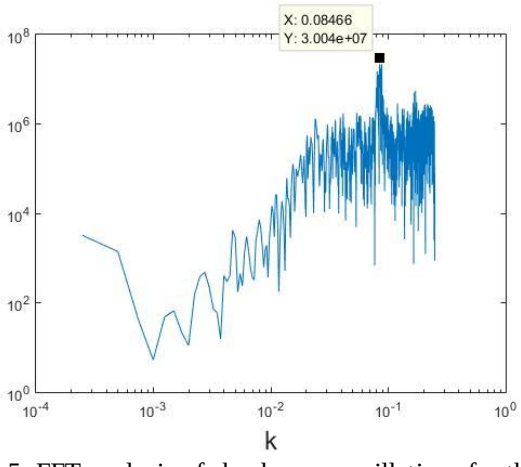

Fig. 5. FFT analysis of shockwave oscillations for the 4° AoA case.

Other than a weak secondary peak at the first harmonic of the main frequency (*k = 0.17*), there are no other peaks in the spectrum.

Figure 6 presents results for the 2° AoA case. The FFT peak, at *k = 0.08373* is very close to the one detected at 4°, corresponding to a frequency of 86,25Hz. Its energy, however, is about 57% of its 4° counterpart. There are no other peaks.

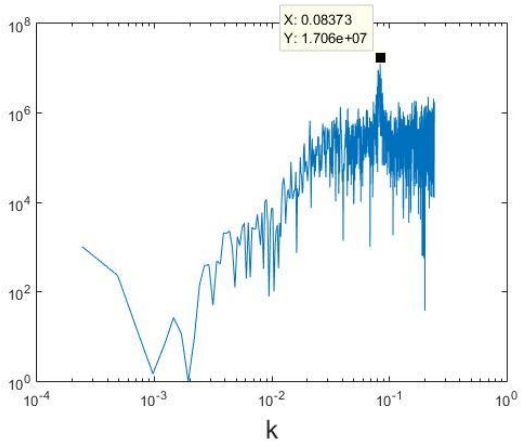

Fig. 6. FFT analysis of shockwave oscillations for the 2° AoA case.

Previous investigations suggest that there is a direct relation between the distance of the mean shockwave position to the trailing edge and shockwave oscillation frequency [23]. The closer to the trailing edge, the higher the frequency. Therefore, the proximity between measured frequencies for 2° and 4° is not surprising, considering that the mean shockwave position, at *x/c =0,45* for 2° and *x/c = 0,43* for 4°, is very close. The 2° case, presenting a shockwave slightly closer to the trailing edge, has a slightly higher oscillation frequency.

Besides the oscillation frequencies reported in this paper, it is possible that a high frequency component is present in the oscillation pattern, as reported by Brion et al. for a supercritical airfoil under laminar flow. The Data presented in figures 5 and 6 was acquired at 500Hz. Data acquisition rates of 2000Hz and 3000Hz presented similar results, only noisier due to reduced camera exposition and, therefore, lower image intensity. If this high-frequency component has a similar Strouhal number for a NACA0012, it would be above our highest acquisition frequency and, therefore, undetectable by a simple FFT analysis.

Visualization of time-resolved whole airfoil pressure fields indicate that shock oscillations are of Tiejdman type A, characterized by almost sinusoidal shock motion within a well-defined oscillation region. Figure 7 presents the shock region pressure fluctuations time series after applying a 50-150Hz band pass filter.

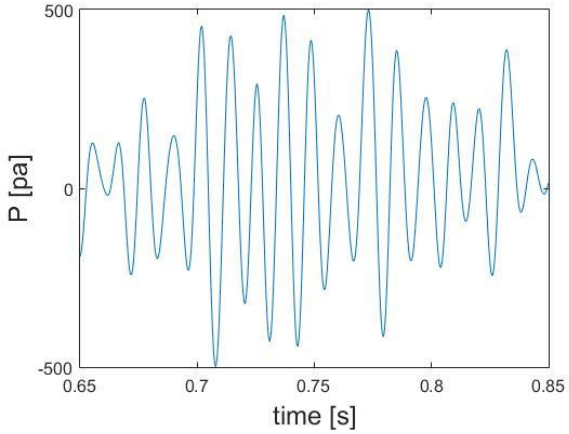

Fig. 7. A sample of pressure fluctuations at the shock region for the 4° AoA case.

Figure 8 presents the phase difference between the mean shock position and various points along the chord at shockwave oscillation frequency. This was calculated using Cross Power Spectral Density (CPSD). In addition, the profile of pressure fluctuations for this case is also represented, in order to facilitate the identification of regions of interest.

In total, six regions with different types of interactions with the shockwave-induced pressure oscillations can be identified. They are delimited by letters A to E in figure 8. The region between C and D, corresponding to *x/c = 0,38* to *x/c = 0,46* delimit the main shock oscillation region and, naturally, every measured point within this region is in phase with the shockwave induced pressure oscillations. The region between A and B, *x/c = 0,21* to *x/c = 0,30*, corresponds to the first leg of the lambda shockwave, and, despite a greater degree of dispersion, is also in phase with the shockwave oscillations. This indicates that the shockwave is moving as a whole, supporting the observations of Brion et al. [22] according to

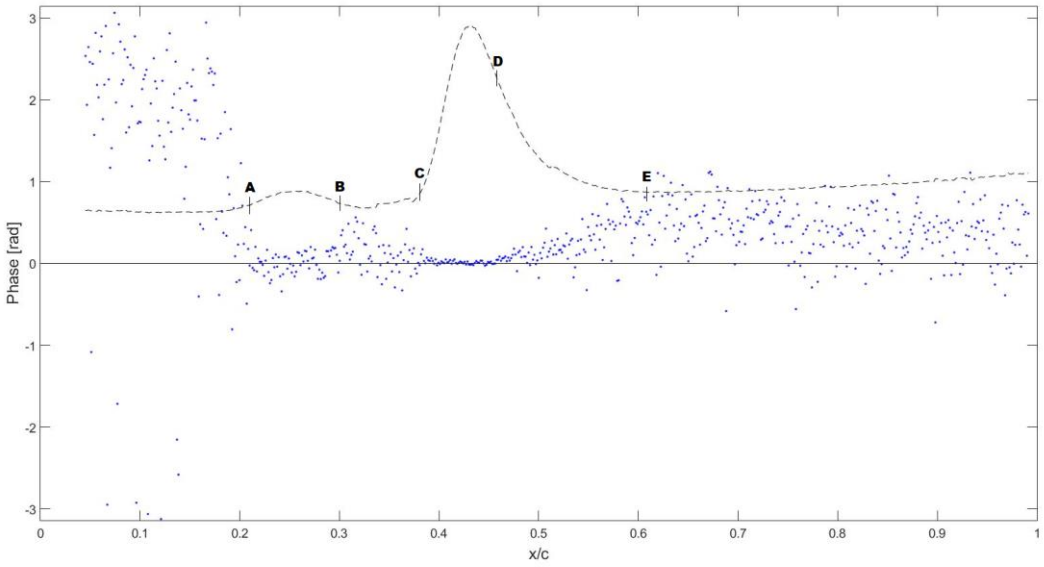

Fig. 8. Phase shift between pressure fluctuations at the mean shockwave position and at various points along the chord, measured at the shock oscillation reduced frequency of $k = 0{,}8466$, AoA 4°. The dashed line is the chordwise pressure fluctuations profile.

whom the low-frequency component of laminar buffet corresponds to the movement of the entire shock structure. Between regions C and D, a laminar separation bubble is often present, and data points in this region present stronger dispersion when compared to their vicinity. The bubble likely acts as a buffer, reducing the influence of the shock oscillations within this region. The fact that the region between points A and B, upstream of the bubble are in phase with the shock oscillations indicate that the mechanism the leads to shock motion also operates outside the boundary layer region.

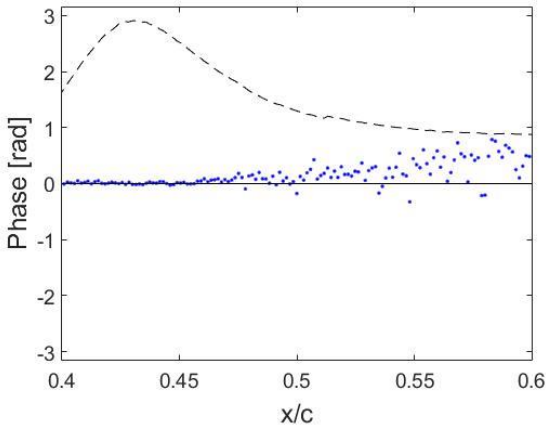

Fig. 9. A closer look at phase shift values between points D and E.

Upstream of point A, phase rapidly shifts to values around 120°, albeit with high variability. The fact that they are not completely random, however, indicates a certain degree of influence from the shock oscillations. A similar, but smoother increase in phase shift and dispersion is observed between points D and E, $x/c = 0{,}46$ to $x/c = 0{,}61$. This region is still under direct influence from the shockwave oscillation, as indicated by the significant values of P_{rms}, but it becomes weaker further downstream. Figure 9 provides a closer look at this region.

After point E, there is no discernible variation in phase shift, which remains centered around 20° and with high variability.

4 Conclusions

The measurement system based on the polymer-ceramic fast-response pressure sensitive paint was able to capture shockwave oscillations accurately, while the polymer-based TurboFIB failed due to the thickness of the paint layer being too high. Measurements with acquisition frequencies of 500Hz, 2000Hz and 3000Hz were performed and presented similar results. A proper evaluation of the accuracy of these results, however, is hampered by the

scarcity of data on shockwave oscillations under laminar flow and the lack of alternative pressure sensors with adequate time response.

Shockwave oscillations were detected for two of the three test conditions. At 2° of angle of attack, fluctuations were of small amplitude and intensity, indicating incipient buffet. At 4°, oscillations were stronger, both in intensity and amplitude, which indicates this condition is well within buffet boundaries. Clear oscillation frequencies could be measured at both cases and were very close. This similarity is due to almost identical mean shockwave positions.

Finally, phase shift information from CPSD analysis revealed six regions of interaction with the shockwave-induced pressure fluctuations. The first, extending from the leading edge up to the first leg of the lambda shockwave, is shifted 120° from the shock oscillations, with a high level of dispersion. At the region where the first leg oscillates, fluctuations are in phase. Between the first and second legs of the shock, where a recirculation bubble is often present, phase shift values present a higher degree of dispersion. At the main shockwave oscillation region, fluctuations are tightly in phase, as expected. Downstream of the shock, the phase gradually shifts to values close to 20°, with increasing variance. At x/c near 0,61, both phase shift and dispersion become somewhat constant and remain so until the trailing edge.

References

[1] Lee B. Self-sustained shock oscillations on airfoils at transonic speeds. *Progress in Aerospace Sciences*, Vol 37, No. 2, pp 147-196, 2001.

[2] Edwards J, Schuster D, Spain C, Keller D, Moses R. *MAVRIC flutter model transonic limit cycle oscillation test.* NASA technical paper TM-2001-210877, 2001.

[3] Yang Z, Dang H. Buffet Onset Prediction and Flow Field Around a Buffeting Airfoil at Transonic Speeds. *Proceedings of the 51st AIAA Structures, Structural Dynamics, and Materials Conference*, Orlando, USA, 2011.

[4] Bhamidipati K K, Reasor D A R, Pasiliao C L. Unstructured Grid Simulations of Transonic Shockwave-Boundary Layer Interaction-Induced Oscillations. *Proc 22nd AIAA Computational Fluid Dynamics Conference*, Dallas, USA, AIAA 2015-2287, 2015.

[5] Hilton W F, Fowler R G. Photographs of Shock Wave Movement. *NPL Reports and Memoranda No. 2692*. National Physical Laboratories, 1947.

[6] McDevitt J, Okuno A. *Static and Dynamic Pressure Measurements on a NACA 0012 Airfoil in the Ames High Reynolds Number Facility.* NASA technical paper No. 2485, 1985.

[7] Pearcey H H. Some Effects of Shock-Induced Separation of Turbulent Boundary Layers in Transonic Flow Past Aerofoils. *NPL Reports and Memoranda No. 3108*. National Physical Laboratories, 1955.

[8] Mundell A R G, Mabey D G. Pressure Fluctuations Caused by Transonic Shock/Boundary-layer Interaction. *Aeronaut Journal*, Vol. 264, No. 81, 1986.

[9] Tijdeman H. Investigation of the Transonic Flow Around Oscillating Airfoils. *NLR Technical Report 77090 U*. National Aerospace Laboratory, The Netherlands, 1977.

[10] Delery J, Marvin G. *AGARDograph No. 280 Shock-Wave Boundary Layer Interactions*. NATO AGARD-AG-280, 1986.

[11] Ackeret J, Feldmann F, Rott N. Investigation of Compression Shocks and Boundary Layers in Gases Moving at High Speed. *NACA Technical Memorandum No 1113*. USA, 1947.

[12] Dor J B, Mignosi A, Seraudie A, Benoit B. Wind tunnel studies of natural shock wave separation instabilities for transonic airfoil tests. *Symposium Transsonicum III*. pp. 417–427. Springer, 1989.

[13] Leite H, Avelar A, Falcão Filho J, Silva A. Experimental study of Shockwave Formation Patterns Over an Airfoil on Laminar Flow and Its Relationship with Boundary Layer Transition. *Proceedings of the 47th AIAA Fluid Dynamics Conference*, Denver, USA, 2017.

[14] Falcão Filho J, Avelar A, Reis M. Historical Review and Future Perspectives For Pilot Transonic Wind Tunnel of IAE. *Journal of Aerospace Technology and Management*, Vol. 1, No. 1, pp. 19-27, 2009.

[15] Leite H, Avelar A, Francisco C P F, Sakaue H. Fast-PSP Based Investigation of Dynamic Shockwave Formation. *Proc 2018 AIAA Science and Technology Forum and Exposition*. Kissimmee, EUA, 2018.

[16] Crafton J, Forlines A, Palluconi S, Hsu K, Campbell C, Gruber M. Investigation of transverse jet injections in a supersonic crossflow using fast-responding pressure-sensitive paint. *Exp Fluids*, Vol. 56, No. 2, 2015.

[17] Gregory J, Sullivan J. Effect of Quenching Kinetics on Unsteady Response of Pressure-Sensitive Paint. *AIAA Journal*, Vol. 44, No. 3, 2006.

[18] Jahanmiri, M. *Pressure Sensitive Paint: the Basics & Applications***.** Research Report, Chalmers University of Technology, Goteborg, Sweden, 2011.

[19] Liu T, Sullivan J P. *Pressure and Temperature Sensitive Paints.* Springer-Verlag, Berlin - ISBN 3-540-22241-3, 2005.

[20] Gregory J W, Sakaue H, Liu T, Sullivan J P. Fast Pressure-Sensitive Paint for Flow and Acoustic Diagnostics. *Annu.Rev.Fluid Mech.* Vol. 46, pp. 303–30, 2014.

[21] Goffert B, Ortega M, Falcão J B P. A Numerical and Experimental Study of an Airfoil in a Transonic Wind Tunnel. *Proc 51st AIAA Aerospace Sciences Meeting.* Grapevine, USA, AIAA 2013-0645, 2013.

[22] Brion V, Abart J C, Paillart P. Laminar Buffet and Flow Control. *Proc European Conference for Aeronautics and Space Sciences*. Milan, Italy. EUCASS2017-61, 2017.

[23] Xiong J, Liu F, Luo S. Computation of NACA0012 Airfoil Transonic Buffet Phenomenon With Unsteady Navier-Stokes Equations. *Proc 50th AIAA Aerospace Sciences Meeting*. Nashville, USA. AIAA 2012-0699, 2012

Copyright Statement